

1 **Observed Impact of Smoke Aerosols on the Stratocumulus-to-Cumulus Transition in**  
2 **the Equatorial Atlantic**

3 **Osinachi F. Ajoku<sup>1\*</sup>, Arthur J. Miller<sup>1</sup>, and Joel R. Norris<sup>1</sup>**

4 1 Scripps Institution of Oceanography, University of California, San Diego, La Jolla, California,  
5 USA

6  
7 Corresponding author: Osinachi Ajoku ([oajoku@ucsd.edu](mailto:oajoku@ucsd.edu))

8 **Key Points:**

9• Transport of smoke aerosols within the equatorial Atlantic impact the stratocumulus to cumulus  
10 transition.

11• Aerosol radiative effects alter lower tropospheric stability and moisture availability throughout  
12 the tropical and subtropical Atlantic.  
13

## 14 Abstract

15 The impact of smoke aerosols on the stratocumulus-to-cumulus transition (SCT) in the equatorial Atlantic is studied  
16 using observation-based data for the month of June. Boundary layer deepening and increasing sea surface  
17 temperatures put the location of the SCT within the Gulf of Guinea. Satellite retrievals indicate that the bulk of  
18 aerosols occurs at 1500m in altitude, either above or below the boundary layer depending on latitudinal position.  
19 Changes in smoke loading over the Gulf of Guinea due to greater transport from regions of biomass burning leads to  
20 increased low-level cloud cover and lower surface temperatures when aerosol optical depth anomalies exceed 0.1.  
21 Similar results opposite in sign are obtained during lesser transport. Further south, we find significant changes to  
22 cloud top height, tropospheric stability and moisture availability. These effects combine to alter the SCT during  
23 increased loading, which is consistent with previous modeling studies.

## 24 1 Background/Introduction

25 Differential heating due to Earth's axial tilt causes excess energy in the form of shortwave radiation in the tropics  
26 that must be transported poleward. This sets up regions with considerable meridional sea surface temperature (SST)  
27 gradients. In addition, locations with eastern boundary currents that transport cooler waters equatorward coupled  
28 with large-scale subsidence are dominated by persistent stratocumulus decks [Klein and Hartmann, 1993]. As these  
29 decks follow the mean trade wind circulation equatorward, the cloud regime transitions from predominantly  
30 stratocumulus to trade cumulus [Bretherton, 1992; Bretherton and Wyant, 1997; Bretherton et al., 1999; Teixeira et  
31 al., 2011]. A better understanding of this Stratocumulus-to-Cumulus transition (SCT) is important for modelling  
32 cloud interactions in a changed climate.

33  
34 Factors that may potentially influence this transition has been studied using both observations [Albrecht et al., 1995;  
35 Albrecht et al., 2019; Wood et al., 2018] and model simulations [Chung et al., 2012; Sandu and Stevens, 2011]. The  
36 major factors controlling cloud coverage in these transition regions are lower tropospheric static stability (LTS)  
37 [Wood and Bretherton, 2006] and the typical advection of a cloud system over increasing SST. These two factors  
38 have been identified as important for all the ocean basins and they both lead to larger surface latent heat fluxes,  
39 buoyancy fluxes and boundary layer deepening.

40  
41 Aerosols alter earth's radiation budget in three different ways, all of which can contribute to changes in cloud  
42 properties. First, aerosols directly impact the planetary energy balance through the absorption and scattering of  
43 incoming radiation [Ramanathan, 2001; Haywood and Boucher 2000], which is known as the "direct effect".  
44 Second, some aerosols act as cloud condensation nuclei (CCN), thereby influencing cloud droplet size and  
45 consequently the likelihood of coalescence and the accumulation of liquid water and ice in clouds, thus altering  
46 cloud albedo and lifetime [Albrecht, 1989; Ferek et al., 2000; Ghan et al., 2012]. This is the so-called "indirect  
47 effect". Third, solar absorbing aerosols such as black carbon can alter heating rates, the vertical temperature profile,  
48 and atmospheric stability, which can lead to cloud adjustments. The radiation flux associated with this adjustment is  
49 termed the aerosol "semi-direct effect" [Hansen et al., 1997].

50  
51 Observations have been used to understand the influence of smoke aerosols on boundary layer clouds in the  
52 southeastern Atlantic [Painemal et al., 2014; Wilcox, 2010, 2012]. The consensus from such studies is that the  
53 location of the smoke layer relative to the cloud deck ultimately determines the resulting effect. When smoke resides  
54 above the cloud deck, there tends to be a strengthening of the inversion layer and cloud radiative effect whereas  
55 smoke within the boundary layer leads to decreased cloud fraction and increased temperatures within the boundary  
56 layer.

57  
58 There have been few studies that look into how smoke aerosols may impact the SCT [Sandu and Stevens, 2011;  
59 Yamaguchi et al., 2017; Terai et al., 2014; Painemal et al., 2015; Zhou et al., 2015] and fewer studies that use  
60 observations in the Atlantic Ocean. The Atlantic Stratocumulus Transition Experiment-ASTEX [Albrecht et al.,  
61 1995] conducted in 1992 resulted in data leading to a coherent understanding as well the first measurements of its  
62 kind for cloud microphysical properties in the SCT of the northeastern subtropical Atlantic but did not investigate  
63 the impact of smoke aerosols.

64  
65 In the southeastern subtropical Atlantic, there has not been an observational study looking at how aerosols may  
66 impact the SCT. Some studies that use large-eddy simulations (LES) to better understand this phenomenon

67 [Yamaguchi *et al.*, 2015; Zhou *et al.*, 2017] incorporate observed data from the northeastern subtropical Pacific and  
 68 knowledge of smoke aerosols from active fires interacting with stratocumulus clouds off the coast of Southern  
 69 Africa. Both studies find evidence of aerosols impacting the SCT but through contrasting mechanisms and end  
 70 results. Yamaguchi *et al.*, [2015] attribute a delay of the SCT to increased LTS due to aerosol heating above the  
 71 cloud layer, while Zhou *et al.*, [2017] find a hastened transition due to increased cloud droplet number concentration  
 72 and cloud water evaporation.

73  
 74 The scientific questions motivating this study are:

- 75  
 761. Can we clearly see a SCT region where black carbon aerosol emissions impact low-level cloud fraction?  
 772. What are the important mechanisms of black carbon aerosols possibly impacting the spatial structure of the SCT?

78  
 79 Knowing that these transitions occur in all four subtropical ocean basins, not many locations can satisfy the added  
 80 component of solar-absorbing aerosols (black carbon) being present. We have located a region in the equatorial  
 81 Atlantic with various cloud types transitioning from stratocumulus to trade cumulus and even deep convective  
 82 cumulonimbus that have the potential to be influenced by local smoke aerosol emissions. This study will be  
 83 extremely important for designing future field campaigns and testing global climate models (GCMs) abilities to  
 84 simulate the SCT.  
 85

## 86 2 Data Sources and Methods

87 In order to determine the impact of smoke aerosols on cloud structure and precipitation processes, daily-averaged  
 88 data are utilized from a variety of sources (with the exception of aerosol extinction). Utilizing daily intervals of data  
 89 allows for a better sampling resolution as well as capturing mesoscale and synoptic-scale weather processes that  
 90 would not be resolved with monthly data output.

91 Daily aerosol optical depth (AOD) for the years 2003-2015 are obtained from Modern-Era Retrospective analysis  
 92 for Research and Applications, Version 2 (MERRA-2) at 0.5°x0.625° resolution [GMAO, 2015]. Having missing  
 93 AOD data can lead to large errors when undergoing statistical analysis. Using reanalysis data reduces such errors as  
 94 data not captured by observations are assimilated using a numerical algorithm to create a synthesized estimate of the  
 95 state of the climate system (Bengtsson *et al.*, 2004). Observations, such as the aerosol index and aerosol absorption  
 96 optical depth obtained from the Ozone Monitoring Instrument (OMI) measurements and aerosol retrievals from the  
 97 AEROSOL ROBOTIC NETWORK (AERONET) [Buchard, *et al.*, 2015] validated the MERRA data obtained from  
 98 reanalysis used in our study. This data is based on a version of the NASA Goddard Earth Observing System version  
 99 5 (GEOS5) model that is radiatively coupled to the Goddard Chemistry, Aerosol, Radiation, and Transport  
 100 (GOCART) aerosol module and includes assimilation of observations from satellites.

101  
 102  
 103 To analyze the effect of aerosols on cloud cover, we obtained cloud coverage data during the study period from  
 104 Clouds and the Earth's Radiant Energy System (CERES) data, which is available, daily-averaged, at 1-degree  
 105 resolution [Doelling *et al.*, 2013; Doelling *et al.*, 2016]. This data is broken down into 4 vertical cloud levels (low  
 106 [surface-700mb], mid-low [700mb-500mb], mid-high [500mb-300mb] and high [300mb-tropopause]). Cloud  
 107 properties are determined using simultaneous measurements by other EOS and S-NPP instruments such as the  
 108 Moderate Resolution Imaging Spectroradiometer (MODIS) and the Visible and Infrared Sounder (VIRS).

109  
 110 High resolution (0.25°x0.25°) daily SST data is provided by the National Oceanic and Atmospheric  
 111 Administration's (NOAA) Earth System Research Laboratory (ESRL) Physical Sciences Division [Reynolds *et al.*,  
 112 2007]. NOAA's 0.25° daily Optimum Interpolation Sea Surface Temperature (OISST) data is compiled from  
 113 observational platforms taking into account bias adjustments.

114  
 115 Daily wind, temperature, specific humidity, convective available potential energy (CAPE), and cloud liquid water  
 116 content data at 0.75° by 0.75° resolution were obtained at multiple pressure levels ranging from the surface to  
 117 500hPa from the European Centre for Medium-Range Weather Forecasts (ECMWF) reanalysis product [Berrisford  
 118 *et al.*, 2011] at a local time of 6 A.M. UTC. This is consistent with the analysis of Tosca *et al.*, [2015], who studied

119 the changes in cloud fraction associated with variability in fire emissions and compared meteorological variables in  
120 control and high fire scenes using ECMWF reanalysis at a 6 A.M. local time to better understand the influence of  
121 mesoscale dynamics. Furthermore, mid-level clouds have been found to dominate cover over West Africa during the  
122 monsoon season early in the morning [*Bourgeois et al.*, 2018].

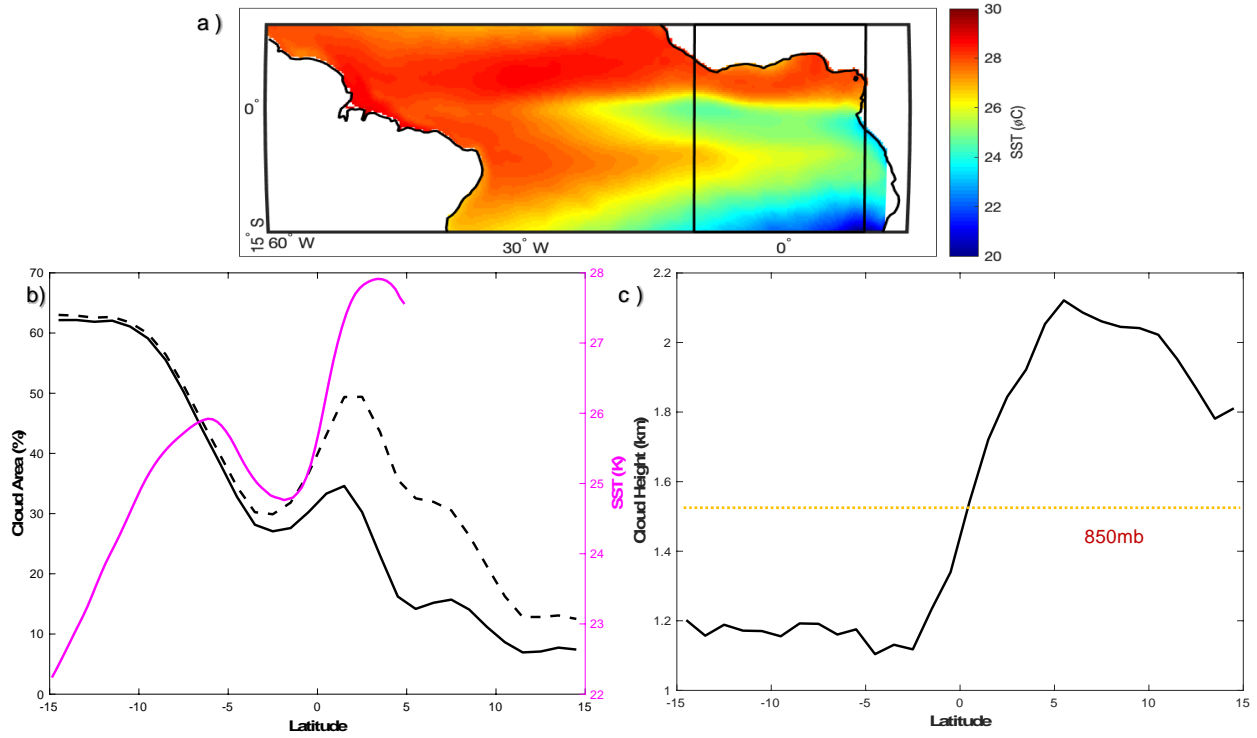
123  
124 In order to quantify the magnitude and location of anomalous changes in rainfall, daily data at 1-degree resolution is  
125 obtained from the Global Precipitation Climatology Project, Version 1.2 (GPCP 1.2). All the GPCP products are  
126 produced by optimally merging precipitation estimates computed from microwave, infrared, sounder data observed  
127 on board satellites, and ground-based rain gauge analysis, taking advantage of the strengths of each data type  
128 [*Huffman et al.*, 2016]. These satellite datasets have been validated against rain gauges on land in West Africa,  
129 particularly on sub-monthly time scales [*Nicholson et al.*, 2003].

130 Monthly smoke aerosol extinction coefficients are acquired from NASA's Cloud-Aerosol Lidar and Infrared  
131 Pathfinder Satellite Observation (CALIPSO) platform for the years 2003-2015 using the Cloud-Aerosol Lidar with  
132 Orthogonal Polarization (CALIOP) instrument. CALIPSO lidar level 3 aerosol data product reports monthly mean  
133 profiles of aerosol optical properties on a 2°x5° spatial grid [*Winker, 2015*] and 60m resolution in the vertical  
134 direction. We use monthly data because the return time between overpasses is too long at daily intervals.

135 Data analysis is conducted for June, representing monsoon onset as well as the establishment of a cold tongue in the  
136 eastern equatorial Atlantic Ocean as the intertropical convergence zone (ITCZ) migrates northward, intensifying  
137 trade winds and creating large meridional SST gradients. Our study region comprises of the boundary between  
138 15°N-15°S and 10°W-10°E (Figure 1a). Also, to note, SST's decrease 2°C in the Gulf of Guinea (GoG) from the  
139 beginning to end of June. As a result, all data used in this study are detrended by the mean monthly June trend to  
140 remove variability arising solely from the seasonal cycle.

141 For each of the 13 years, the 30 days in each June were classified into pentiles according to the magnitude of AOD  
142 averaged between 5°N-5°S and 10°W-10°E in the GoG for that day. The top and bottom pentiles aggregated from  
143 each June resulted in 78 days that are referred to as "clean" (lowest AOD) and "dirty" (highest AOD) days. All dates  
144 associated with these dirty and clean days are averaged together to create composites that track how aerosol loading  
145 evolves with other meteorological variables of interest. Trends are then removed from composited data to reveal  
146 detrended, anomalous changes. By utilizing this method, we attempt to determine which variables are impacted by  
147 variations in aerosol transport. Statistical significance of results was determined by the 95% confidence interval  
148 according to a 2-tailed Student's t-test accounting for serial correlation by using the effective sample size,  $n(1-$   
149  $r_1)(1+r_1)^{-1}$ , where  $n$  is the number of days and  $r_1$  is the lag-1 autocorrelation coefficient leading to ~3 day  
150 decorrelation time.

151



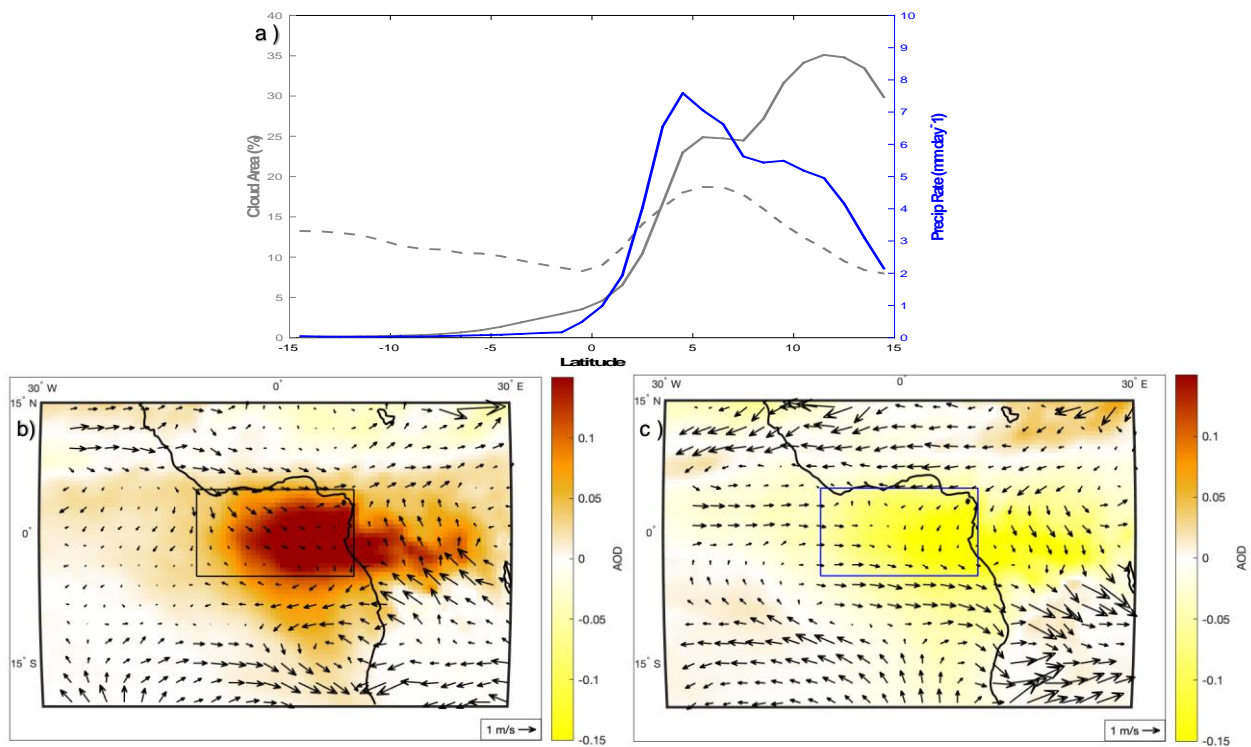
152  
153  
154  
155  
156

**Figure 1.** (a) Climatological June SST, (b) zonally-averaged low cloud area fraction and SST and (c) corresponding cloud top height for the years 2003-2015. The black box in (a) represents longitudinal boundaries used to average data in (b) and (c) as well as subsequent figures. Dashed black lines in (b) represent cloud area fraction accounting for obscuration from high level clouds.

157 **3 Results**158 **3.1. Study Region Overview**

159 For the month of June, climatological conditions in the Eastern equatorial Atlantic are excellent for studying the  
 160 SCT. Between the ITCZ migration and trade wind intensification, a large, meridional SST gradient sets up a  
 161 corresponding cloud structure aloft. Starting in the southern subtropical Atlantic moving equatorward, we see an  
 162 inverse relationship between increasing SST and decreasing low-level cloud fraction (Figure 1b). Of particular  
 163 interest, we notice two locations where cloud fraction decreases to half the value it had farther south (7°S-3°S and  
 164 1°N-5°N). We note that this decrease is not as pronounced when accounting for obscuration from high-level clouds.  
 165 Within the Gulf of Guinea (GoG), we examine the structure of cloud top height and find a ~700m increase (Figure  
 166 1c) in the same location that the cloud fraction decreases. We believe this is where the boundary layer deepens due  
 167 to increasing SST in GoG and where the stratocumulus deck transitions into cumulus clouds. Further aloft, increases  
 168 in higher level clouds (Fig 2 a) occur within the GoG in addition to precipitation rates rising to a maximum.

169



170

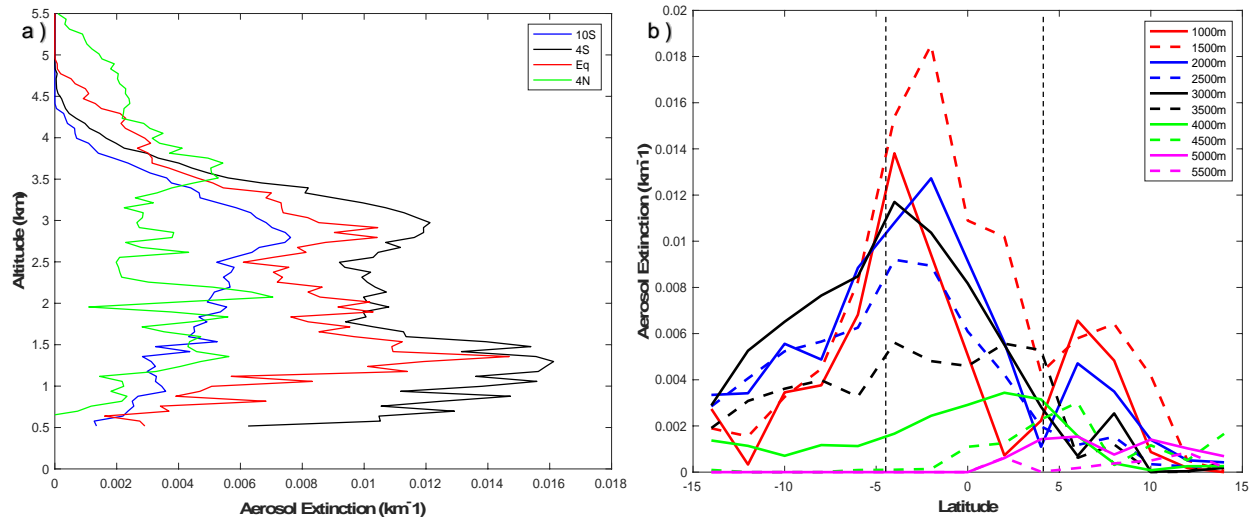
171 **Figure 2.** (a) Climatological, zonally-averaged mid-high (gray, dashed) and high (gray, solid) cloud fraction overlain with  
 172 precipitation rates for the years 2003-2015, see Figure 1 for averaging area. AOD and 850 hPa wind anomalies for dirty (b) and  
 173 (c) clean days during the same time period. Rectangular boxes in (b) and (c) represent averaging areas for composite analysis.

174

175 **3.2. Aerosol-Low Cloud-SST Feedback**

176 In order to understand aerosol-cloud interactions, first we must visualize at what altitude smoke aerosols are located.  
 177 Long-term mean vertical aerosol extinction profiles representing locations in our study region are shown in figure  
 178 3a. We see the largest values at 4°S and the equator at an altitude just below 1500 meters. This extinction maximum  
 179 occurs above the low cloud top height (Fig 1c). Further north, we notice decreases in mean extinction as aerosols  
 180 enter the boundary layer. Regardless of location, values taper toward 0 near 5.5 km. Figure 3b shows that most of  
 181 the smoke along the Prime Meridian is located between 1000m-3000m specifically where AOD anomalies exceed  
 182 0.1 (~25% of the monthly mean) on dirty and clean days (Fig 2 b, c).

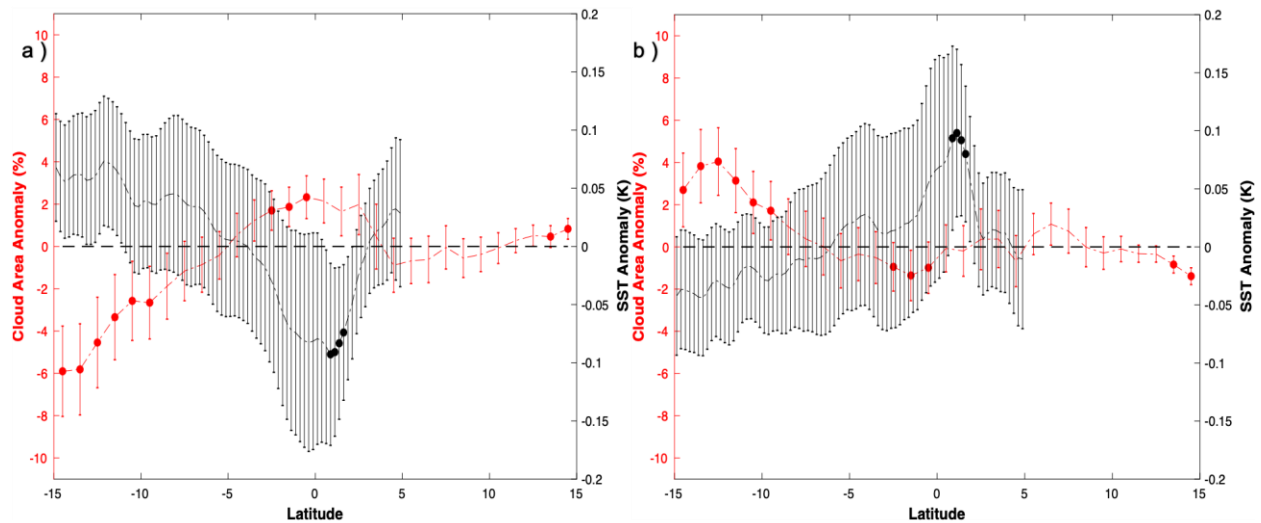
183



184

185 **Figure 3.** (a) Long-term mean single point and (b) zonally-averaged smoke aerosol extinction profiles for the month of June  
 186 (2003-2015). Data in panel (a) represent values along the Prime Meridian. Dotted lines in panel (b) represent the boundary where  
 187 AOD anomalies exceed 0.1. See Figure 1 for averaging area.

188 During dirty/clean smoke episodes, we find evidence of increased/decreased low-cloud fraction specifically within  
 189 the equatorial Atlantic cold tongue zone and within the area where maximum aerosol loading occurs. As low cloud  
 190 fraction increases, it is possible the amount of shortwave radiation reaching the ocean surface diminishes as is  
 191 reflected by changes in SST (Fig 4). It is difficult to discern whether this is due to the cloud radiative effect (CRE)  
 192 or aerosol radiative effect (ARE) with pure observations. However, we find positive low cloud fraction anomalies  
 193 where cloud top heights reach a minimum near the cold tongue. Figure 3b shows that the bulk of smoke aerosols  
 194 resides above this height. Thus, our results are in agreement with previous studies that find evidence of  
 195 stratocumulus thickening above smoke layers with enhanced loading [Wilcox, 2010; Wilcox, 2012; Li et al., 2013].  
 196 As smoke travels north or south within the boundary layer, cloud fraction decreases, as found in Zhang and Zuidema  
 197 [2019, in review]. Significant decreases are found south of 5°S as recent evidence shows that the boundary layer is  
 198 often smoky especially in June [Zuidema et al., 2018], although we can rule out the influence of meteorological  
 199 parameters [Adebiyi and Zuidema, 2018].



200

201

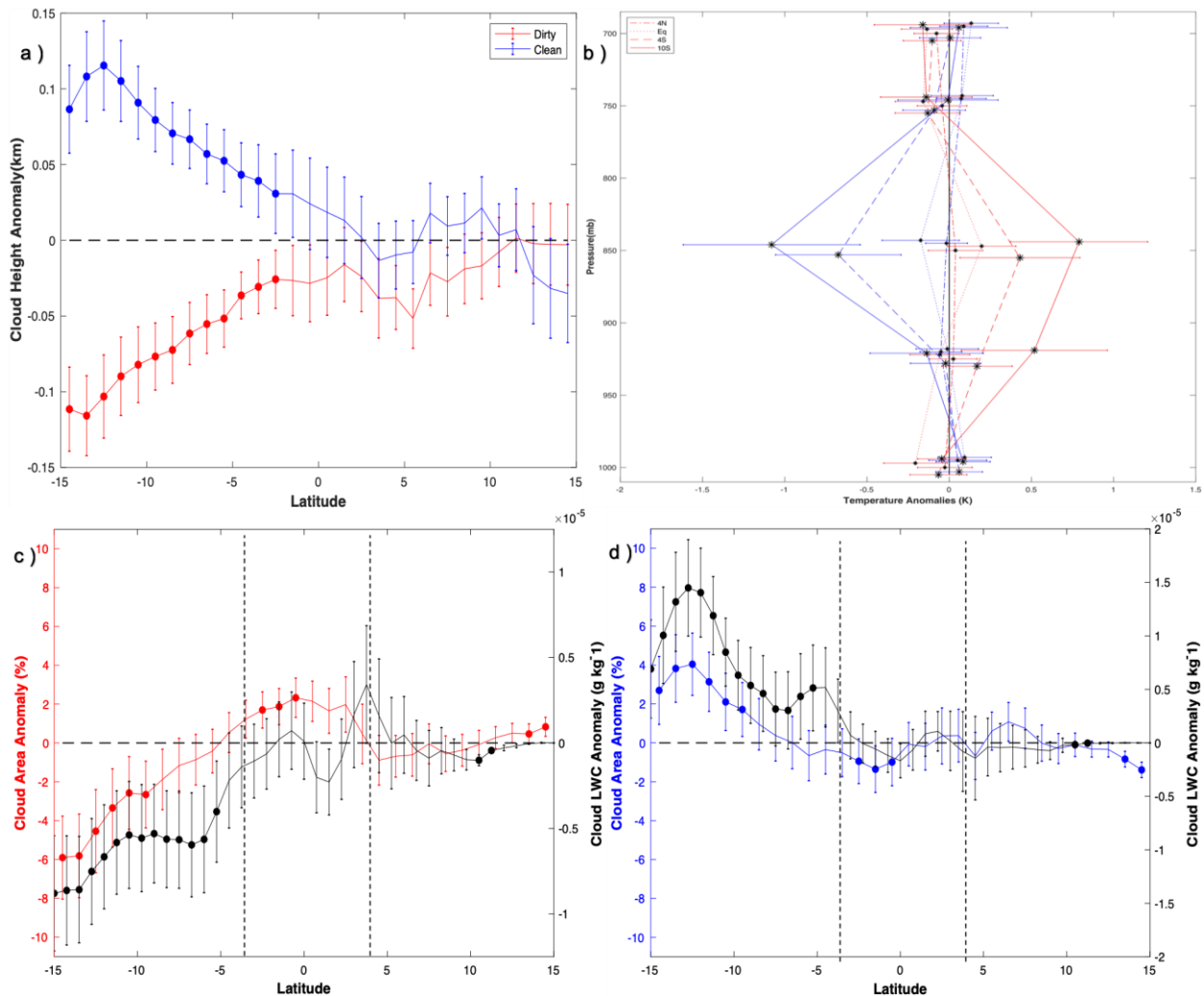
202

203

**Figure 4.** Zonally averaged low cloud area fraction and SST anomalies for (a) dirty and (b) clean smoke episodes. See Figure 1 for averaging area. Error bars range 1 standard error and filled circles represent locations where the difference between sampled means exceed the 95% confidence level.

204 **3.3. Stability vs. Moisture Aloft**

205 *Yamaguchi et al.*, [2015] find that smoke aerosols delay the SCT by strengthening of the inversion layer. In  
 206 accordance with this study and others that look at LTS as a controlling factor for low cloud amount within SCT  
 207 regions [*Wood and Bretherton, 2006; Sandu and Stevens, 2011*], we examined changes in potential temperature ( $\theta$ )  
 208 profiles and cloud top height anomalies (Fig 5). Here, we can clearly see the effects of anomalous smoke loading on  
 209 atmospheric stability. During dirty smoke episodes, we find significant decreases in low-level cloud top height  
 210 between 25-100 meters from the cold tongue southwards (Fig 5a). By analyzing  $\theta$  anomalies along the Prime  
 211 Meridian transect, we can infer where aerosols impact stability within the lower troposphere (Fig 5b). As expected,  
 212 the largest response occurs near 850hPa, which corresponds to ~1500m above sea level (Fig 1c). In the subtropics  
 213 (10°S and 4°S), we find the largest changes in cloud height and  $\theta$  anomalies although smoke aerosol extinction  
 214 values do not vary much between 750m-4000m. Further north, these changes are less pronounced. We note  
 215 significant surface cooling during dirty episodes, particularly at the equator where low cloud anomalies peak.



216  
 217 **Figure 5.** Anomalous changes in meteorological variables representing atmospheric stability and moisture: (a) cloud top height,  
 218 (b)  $\theta$  at various latitudes and cloud liquid water content at 850hPa for dirty(c) and clean(d) conditions. Data plotted in panel b are  
 219 taken along the Prime Meridian. Panels c and d contain dotted lines representing the boundary where AOD anomalies exceed 0.1.  
 220 See Figure 1 for averaging area. Error bars range 1 standard error and filled circles represent locations where the difference  
 221 between sampled means exceed the 95% confidence level.

222 Using a large eddy simulation (LES), *Zhou et al.*, [2017] find a hastened SCT linked to increased cloud droplet  
223 number concentration (due to smoke aerosols) that leads to faster evaporation of cloud water which enhances  
224 entrainment. Their complementary experiments that included additional moisture aloft, which is believed to  
225 accompany biomass burning plumes relative to surrounding air [*Adebisi et al.*, 2015], revealed a more hastened  
226 SCT. In their study, absorbing aerosols above the cloud layer strengthens the inversion and reduces boundary layer  
227 height, in agreement with our findings. However, as aerosols enter into the boundary layer, they find that enhanced  
228 entrainment of surrounding warm, dry air reduces cloud cover. North of the equator, we observe low cloud cover  
229 and cloud liquid water content (CLWC) at 850hPa slightly change simultaneously (Fig 5 c-d) where smoke enters  
230 into the boundary layer (Fig 1c) but are not significant. During dirty episodes, we find 10-20% ( $0.1-0.2 \text{ g kg}^{-1}$ ) of  
231 moisture increases at 850hPa within our region of max AOD loading (Fig 5d) relative to recent observational studies  
232 [*Adebisi et al.*, 2015; *Haywood et al.*, 2003]. However, those studies occurred in the southern Atlantic so our  
233 estimates may not be directly comparable.

## 234 **4 Conclusions**

235 Using observational data, we have isolated a mechanism for modulating the SCT in the equatorial Atlantic that has  
236 not yet been discussed in the literature. This transition is located within the GoG and thus we conducted our AOD  
237 composite analysis at this location.

238 In the subtropical Atlantic ( $15^{\circ}\text{S}-5^{\circ}\text{S}$ ), we attribute reductions in cloud cover during dirty conditions to smoke  
239 mixing within the boundary layer (Fig3b), possibly reflecting a boundary layer positive semi-direct effect [*Zhang*  
240 *and Zuidema*, 2019, in review]. Within the equatorial Atlantic ( $4^{\circ}\text{S}-2^{\circ}\text{N}$ ), elevated smoke levels lead to increases (1-  
241 2%) in low cloud cover along with decreases in SST ( $\sim 0.1\text{K}$ ) and potential temperature ( $\sim 0.2\text{K}$ ) at the surface. Also,  
242 cloud top heights decrease 20-100m, consistent with *Deaconu et al.*, 2019. Boundary layer deepening reflected by  
243 increases in cloud top height (Fig 1c) within the GoG allow for smoke to mix and reduce low cloud cover between  
244  $0^{\circ}-5^{\circ}\text{N}$ , agreeing with hastened SCT from model results [*Zhou et al.*, 2017]. Anomalous 850hPa winds (Fig 2b) do  
245 not reflect a pattern that would control both aerosol and cloud structures.

246 We attribute the switch from less low cloud for dirty conditions south of the cold tongue to more low clouds over the  
247 cold tongue to special air-sea interactions unique to this region. In the subtropics, trade winds advect the boundary  
248 layer over increasing SST's, which favors upward moisture flux from the surface to sustain cloud formations. Here,  
249 aerosol heating in the boundary layer can cause the clouds to evaporate. In contrast, when the boundary layer  
250 reaches the cold tongue, the atmosphere develops near-surface stratification which cuts off the upward moisture flux  
251 needed to sustain clouds from dry air entrainment of the free troposphere. Here, it is possible that aerosol heating  
252 may increase stratification in the upper part of the boundary layer which would reduce dry air entrainment and lead  
253 to longer lasting clouds.

254 Our study region offers more possibilities for research as we see cumulus clouds transitioning into deep-convective  
255 clouds within the GoG. Aerosols do not ascend high enough to have a direct influence on high-level clouds but may  
256 do so indirectly via hastening of the SCT and boundary layer moisture adjustments below. Subsequent changes in  
257 higher-level clouds and precipitation are small, but still worthy to note.

258 We acknowledge that this research relies on observations and so may be subjected to uncertainties associated with  
259 satellite data. It is our hope that these findings will serve as a foundation for designing future field campaigns and  
260 testing modeling studies that investigate the SCT.

## 261 **Acknowledgments, Samples, and Data**

262 All data supporting the conclusions of this research study are available through the references mentioned in the data  
263 sources and methods sections.

264 This research forms a part of the Ph.D. dissertation of OA, who was supported by a National Science Foundation  
265 Graduate Research (DGE-1650112), UC Dissertation Year and San Diego Foundation Fellowships. The National  
266 Science Foundation Earth System Modeling Program (OCE1419306) provided additional funding that supported  
267 this research. We thank Prof. Paquita Zuidema for many constructive comments and suggestions on our research  
268 results.

## 269 **References**

- 270  
271 Adebisi, A. A., Zuidema, P., & Abel, S. J. (2015). The convolution of dynamics and moisture with the presence of  
272 shortwave absorbing aerosols over the southeast Atlantic. *Journal of Climate*, 28(5), 1997-2024.  
273  
274 Adebisi, A. A., & Zuidema, P. (2018). Low cloud cover sensitivity to biomass-burning aerosols and meteorology  
275 over the southeast Atlantic. *Journal of Climate*, 31(11), 4329-4346.  
276  
277 Albrecht, B (1989), Aerosols, cloud microphysics, and fractional cloudiness, *Science*, 245, 1227-1230,  
278 doi:10.1126/science.245.4923.1227  
279  
280 Albrecht, B. A., Bretherton, C. S., Johnson, D., Scubert, W. H., & Frisch, A. S. (1995). The Atlantic stratocumulus  
281 transition experiment—ASTEX. *Bulletin of the American Meteorological Society*, 76(6), 889-904.  
282  
283 Albrecht, B., Ghate, V., Mohrmann, J., Wood, R., Zuidema, P., Bretherton, C., ... & Sarkar, M. (2019). Cloud  
284 System Evolution in the Trades (CSET): Following the evolution of boundary layer cloud systems with the NSF–  
285 NCAR GV. *Bulletin of the American Meteorological Society*, 100(1), 93-121.  
286  
287 Bengtsson, L., Hagemann, S., & Hodges, K I (2004) Can climate trends be calculated from reanalysis  
288 data?. *Journal of Geophysical Research: Atmospheres*, 109(D11)  
289  
290 Berrisford, P, Dee, D, Poli, P, Brugge, R, Fielding, K, Fuentes, M, ... & Simmons, A (2011) The ERA-  
291 Interim archive, version 2.0  
292  
293 Bourgeois, E., Bouniol, D, Couvreur, F, Guichard, F, Marsham, J H, Garcia-Carreras, L, ... &  
294 Parker, D J (2018) Characteristics of mid-level clouds over West Africa. *Quarterly Journal of the*  
295 *Royal Meteorological Society*, 144(711), 426-442  
296  
297 Bretherton, C. S. (1992). A conceptual model of the stratocumulus-trade-cumulus transition in the subtropical  
298 oceans. In *Proc. 11th Int. Conf. on Clouds and Precipitation*(Vol. 1, pp. 374-377). International Commission on  
299 Clouds and Precipitation and International Association of Meteorology and Atmospheric Physics Montreal, Quebec,  
300 Canada.  
301  
302 Bretherton, C. S., & Wyant, M. C. (1997). Moisture transport, lower-tropospheric stability, and decoupling of cloud-  
303 topped boundary layers. *Journal of the atmospheric sciences*, 54(1), 148-167.  
304  
305 Bretherton, C. S., Krueger, S. K., Wyant, M. C., Bechtold, P., Van Meijgaard, E., Stevens, B., & Teixeira, J. (1999).  
306 A GCSS boundary-layer cloud model intercomparison study of the first ASTEX Lagrangian experiment. *Boundary-*  
307 *Layer Meteorology*, 93(3), 341-380.  
308  
309 Buchard, V, da Silva, A M, Colarco, P R, Darmenov, A, Randles, C A, Govindaraju, R, ... & Spurr,  
310 R (2015) Using the OMI aerosol index and absorption aerosol optical depth to evaluate the NASA  
311 MERRA Aerosol Reanalysis. *Atmospheric Chemistry and Physics*, 15(10), 5743  
312  
313 Chung, D., Matheou, G., & Teixeira, J. (2012). Steady-state large-eddy simulations to study the stratocumulus to  
314 shallow cumulus cloud transition. *Journal of the Atmospheric Sciences*, 69(11), 3264-3276.  
315

- 316 Deaconu, L. T., Ferlay, N., Waquet, F., Peers, F., Thieuleux, F., & Goloub, P. (2019). Satellite inference of water  
317 vapour and above-cloud aerosol combined effect on radiative budget and cloud-top processes in the southeastern  
318 Atlantic Ocean. *Atmospheric Chemistry and Physics*, 19(17), 11613-11634.  
319
- 320 Doelling, D R, Loeb, N G, Keyes, D F, Nordeen, M L, Morstad, D, Nguyen, C, ... & Sun, M (2013)  
321 Geostationary enhanced temporal interpolation for CERES flux products. *Journal of Atmospheric and*  
322 *Oceanic Technology*, 30(6), 1072-1090  
323
- 324 Doelling, D R, Sun, M, Nguyen, L. T, Nordeen, M L, Haney, C O, Keyes, D F, & Mlynczak,  
325 P E (2016) Advances in geostationary-derived longwave fluxes for the CERES synoptic (SYN1deg)  
326 product. *Journal of Atmospheric and Oceanic Technology*, 33(3), 503-521  
327
- 328 Ferek, R J, Garrett, T, Hobbs, P V, S3.Itrader, S, Johnson, D, Taylor, J P, ... & Albrecht, B A (2000)  
329 Drizzle suppression in ship tracks. *Journal of the Atmospheric Sciences*, 57(16), 2707-2728  
330
- 331 Ghan, S J, Liu, X, Easter, R C, Zaveri, R, Rasch, P J, Yoon, J H, & Eaton, B (2012) Toward a  
332 minimal representation of aerosols in climate models: Comparative decomposition of aerosol direct,  
333 semidirect, and indirect radiative forcing. *Journal of Climate*, 25(19), 6461-6476  
334
- 335 Global Modeling and Assimilation Office (GMAO)(2015) MERRA-2 tavgM\_2d\_int\_Nx:  
336 2d, Monthly mean, Time-Averaged, Single-Level, Assimilation, Vertically Integrated Diagnostics  
337 V5.12.4, Greenbelt, MD, USA, Goddard Earth Sciences Data and Information Services Center  
338 (GES DISC), Accessed [July 7, 2017] 10.5067/FQPTQ4OJ22TL  
339
- 340 Hansen, J., Sato, M., & Ruedy, R. (1997). Radiative forcing and climate response. *Journal of Geophysical*  
341 *Research: Atmospheres*, 102(D6), 6831-6864.  
342
- 343 Haywood, J, & Boucher, O (2000) Estimates of the direct and indirect radiative forcing due to  
344 tropospheric aerosols: A review. *Reviews of geophysics*, 38(4), 513-543  
345
- 346 Haywood, J. M., Osborne, S. R., Francis, P. N., Keil, A., Formenti, P., Andreae, M. O., & Kaye, P. H. (2003). The  
347 mean physical and optical properties of regional haze dominated by biomass burning aerosol measured from the C-  
348 130 aircraft during SAFARI 2000. *Journal of Geophysical Research: Atmospheres*, 108(D13).  
349
- 350 Huffman, G J, Bolvin, D T, & Adler, R F (2016) GPCP version 1.2 one-degree daily precipitation data  
351 set. *Research Data Archive at the National Center for Atmospheric Research, Computational and*  
352 *Information Systems Laboratory, Boulder, CO*  
353
- 354 Klein, S. A., & Hartmann, D. L. (1993). The seasonal cycle of low stratiform clouds. *Journal of Climate*, 6(8), 1587-  
355 1606.  
356
- 357 Li, J., K. von Salzen, Y. Peng, H. Zhang, and x.-Z. Liang (2013), Evolution of black carbon semi-direct radiative  
358 effect in a climate model, *J. Geophys. Res. Atmos.*, 118, 4715-4728, doi:10.1002/jgrd.50327.  
359
- 360 Nicholson, S E, Some, B, McCollum, J, Nelkin, E, Klotter, D, Berte, Y, ... & Noukpozounkou, J N  
361 (2003) Validation of TRMM and other rainfall estimates with a high-density gauge dataset for West  
362 Africa. Part II: Validation of TRMM rainfall products. *Journal of Applied Meteorology*, 42(10), 1355-1368  
363
- 364 Painemal, D., P. Minnis, and M. Nordeen (2015), Aerosol variability, synoptic-scale processes, and their link to the  
365 cloud microphysics over the northeast Pacific during MAGIC, *J. Geophys. Res. Atmos.*, 120, 5122–5139,  
366 doi:10.1002/2015JD023175.  
367
- 368 Painemal, D., S. Kato, and P. Minnis (2014), Boundary layer regulation in the southeast Atlantic cloud microphysics  
369 during the biomass burning season as seen by the A-train satellite constellation, *J. Geophys. Res. Atmos.*, 119,  
370 11,288–11,302, doi:10.1002/2014JD022182.  
371

- 372 Ramanathan, V C P J, Crutzen, P J, Kiehl, J T, & Rosenfeld, D (2001) Aerosols, climate, and the  
373 hydrological cycle. *science*, 294(5549), 2119-2124  
374
- 375 Reynolds, R. W., Smith, T. M., Liu, C., Chelton, D. B., Casey, K. S., & Schlax, M. G. (2007). Daily high-  
376 resolution-blended analyses for sea surface temperature. *Journal of Climate*, 20(22), 5473-5496.  
377
- 378 Sandu, I., & Stevens, B. (2011). On the factors modulating the stratocumulus to cumulus transitions. *Journal of the*  
379 *Atmospheric Sciences*, 68(9), 1865-1881.  
380
- 381 Teixeira, J., Cardoso, S., Bonazzola, M., Cole, J., DelGenio, A., DeMott, C., ... & Karlsson, J. (2011). Tropical and  
382 subtropical cloud transitions in weather and climate prediction models: The GCSS/WGNE Pacific Cross-Section  
383 Intercomparison (GPCI). *Journal of Climate*, 24(20), 5223-5256.  
384
- 385 Tosca, M G, Diner, D J, Garay, M J, & Kalashnikova, O V (2015) Human-caused fires limit  
386 convection in tropical Africa: First temporal observations and attribution. *Geophysical Research*  
387 *Letters*, 42(15), 6492-6501  
388
- 389 Wilcox, E. M. (2010), Stratocumulus cloud thickening beneath layers of absorbing smoke aerosol, *Atmos. Chem.*  
390 *Phys.*, 10(23), 11,769–11,777, doi:10.5194/acp-10-11769-2010.  
391
- 392 Wilcox, E. M. (2012), Direct and semi-direct radiative forcing of smoke aerosols over clouds, *Atmos. Chem. Phys.*,  
393 12(1), 139–149, doi:10.5194/acp-12-139-2012.  
394
- 395 Winker, D. (2015). CALIPSO LID\_L3\_APro\_AllSky-StandardHDF File – Version 3.00. NASA Langley  
396 Atmospheric Science Data Center DAAC. [https://doi.org/10.5067/caliop/calipso/cal\\_lid\\_l3\\_apro\\_allsky-standard-](https://doi.org/10.5067/caliop/calipso/cal_lid_l3_apro_allsky-standard-v3-00)  
397 [v3-00](https://doi.org/10.5067/caliop/calipso/cal_lid_l3_apro_allsky-standard-v3-00)  
398
- 399 Wood, R., & Bretherton, C. S. (2006). On the relationship between stratiform low cloud cover and lower-  
400 tropospheric stability. *Journal of climate*, 19(24), 6425-6432.
- 401
- 402 Wood, R., O, K. T., Bretherton, C. S., Mohrmann, J., Albrecht, B. A., Zuidema, P., ... & Shaw, R. A. (2018).  
403 Ultraclean layers and optically thin clouds in the stratocumulus-to-cumulus transition. Part I: Observations. *Journal*  
404 *of the Atmospheric Sciences*, 75(5), 1631-1652.
- 405
- 406 Yamaguchi, T., G. Feingold, J. Kazil, and A. McComiskey (2015), Stratocumulus to cumulus transition in the  
407 presence of elevated smoke layers, *Geophys. Res. Lett.*, 42, 10,478–10,485, doi:10.1002/2015GL066544.  
408
- 409 Yamaguchi, T., Feingold, G., & Kazil, J.(2017). Stratocumulus to cumulus transition by drizzle. *Journal of*  
410 *Advances in Modeling Earth Systems*,9, 2333–2349. <https://doi.org/10.1002/2017MS001104>  
411
- 412 Zhang, J. and Zuidema, P.: Low cloud reduction within the smoky marine boundary layer and the diurnal cycle,  
413 *Atmos. Chem. Phys. Discuss.*, <https://doi.org/10.5194/acp-2019-448>, in review, 2019.  
414
- 415 Zhou, X., Ackerman, A. S., Fridlind, A. M., Wood, R., & Kollias, P. (2017). Impacts of solar-absorbing aerosol  
416 layers on the transition of stratocumulus to trade cumulus clouds. *Atmospheric Chemistry and Physics*, 17(20),  
417 12725-12742.  
418
- 419 Zhou, X., Kollias, P., & Lewis, E. R. (2015). Clouds, precipitation, and marine boundary layer structure during the  
420 MAGIC field campaign. *Journal of Climate*, 28(6), 2420-2442.  
421
- 422 Zuidema, P., Sedlacek III, A. J., Flynn, C., Springston, S., Delgadillo, R., Zhang, J., ... & Muradyan, P. (2018). The  
423 Ascension Island boundary layer in the remote southeast Atlantic is often smoky. *Geophysical Research*  
424 *Letters*, 45(9), 4456-4465.  
425